Opposite phase changes of precipitation annual cycle over land and ocean under global warming

Fengfei Song[1], Jian Lu*[1], L. Ruby Leung*[1], Fukai Liu[2]

1. Atmospheric Sciences and Global Change Division, Pacific Northwest National Laboratory, Richland, Washington, USA

2. Physical Oceanography Laboratory/CIMST, Ocean University of China and Qingdao National Laboratory for Marine Science and Technology, Qingdao, China

* Corresponding authors: Jian Lu and L. Ruby Leung

Email: jian.lu@pnnl.gov and ruby.leung@pnnl.gov

Fengfei Song: (Orcid-ID: 0000-0002-3004-1749)

L. Ruby Leung: (Orcid-ID: 0000-0002-3221-9467)

Jian Lu: (Orcid-ID: 0000-0001-8245-6930)

Fukai Liu: (Orcid-ID: 0000-0002-0687-9568)

Submitted to ***Geophysical Research Letters***

Keypoints:

1. Precipitation annual cycle shows a phase delay over land but a phase advance over ocean under global warming;

2. The land delay is due to enhanced effective atmospheric heat capacity and the ocean advance is linked to land-ocean rainfall shift in summer;

3. The enhanced and reduced surface temperature annual cycle over ocean versus land contribute to the rainfall shift via energetic constraint.

Abstract

The annual cycle of precipitation is a fundamental aspect of the global water cycle. Climate warming induces amplitude enhancement and phase delay in the zonal-mean tropical precipitation. Here, we report a land-ocean contrast in the phase response of precipitation annual cycle, with a delay over land and an advance over ocean as climate warms. Although two-thirds of the Earth's surface are covered by ocean, land dominates the zonal-mean phase delay, attributable to an increase in the effective atmospheric heat capacity. The phase advance over ocean is associated with a precipitation shift from land to ocean during the peak rainy season. This shift is well constrained by the energetic and related to a land-ocean contrast in the amplitude change of surface temperature annual cycle: seasonally different wind changes enhance this amplitude over ocean, while increased effective atmospheric heat capacity and surface cooling feedback reduce the amplitude over land.

Plain language summary

The seasonal monsoon rainfall provides the water resource for ~40% of the world population, but it has been a longstanding challenge to predict when monsoon rain will arrive, especially at the regional scale. By separating land from ocean, we revealed that the previous finding of seasonal delay of zonal-mean rainfall under warming mainly occurs over land, where most human activities take place, while ocean shows a phase advance. This contrasting phase behavior between land and ocean is shown to be rooted in the first-principle physical constraints related to energy and climate feedbacks, thus confidence is assigned to the differential phase response between the tropical land and ocean under climate warmng.

1. Introduction

Over the annual cycle, the most prominent hydrological feature is the advance and retreat of tropical rainfall following the movement of monsoons and inter-tropical convergence zone (ITCZ). The annual cycle of tropical rainfall is ultimately driven by solar insolation, but its exact evolution is determined by a myriad of factors, including land-ocean distribution, land surface properties and ocean heat fluxes. Global warming is poised to substantially delay the cyclic progression of tropical rainfall, especially over the monsoonal regions (Biasutti and Sobel 2009; Seth et al. 2011 2013; Pascale et al. 2016; Song et al. 2018a) and enhance its amplitude (Chou et al. 2011; Chou and Lan 2012; Huang et al. 2013). The enhanced tropical precipitation annual cycle mainly occurs over ocean and is due to the increase of moisture under global warming as a "wet-get-wetter" response (Held and Soden 2006; Chou et al. 2009). The seasonal delay of tropical rainfall will induce seasonally-dependent subtropical high responses under warming (Song et al. 2018a, b).

In the past decade, the atmosphereic energetic framework (e.g., Kang et al. 2008; Frierson et al. 2013; Schneider et al. 2014; Boos and Korty 2016; Biasutti et al. 2018) has been developed to relate the ITCZ shift to changes in the net energy input and/or the effective atmospheric heat capacity (Song et al. 2018). The causes of the delay are only beginning to be unveiled through the lens of this energetic perspective (Biasutti and Sobel 2009; Song et al. 2018a). Both the seasonal delay of sea surface temperature (SST) and the annual-mean SST warming can lead to a seasonal delay of tropical precipitation (Biasutti and Sobel 2009; Song et al. 2018; Dwyer et al. 2014). The former is attributed to the high-latitude sea ice melting, which boosts the effective heat capacity of the system by exposing the thick ocean mixed layer to the atmosphere (Dwyer et al. 2012; Donohoe and Battisti 2013). The latter can be explained by the increase of the effective atmospheric heat capacity mainly due to the increase in atmospheric moisture with warming, resulting in a more sluggish response of atmosphereic heat transport (AHT) and precipitation to the seasonal solar forcing (Song et al. 2018a; Cronin and Emanuel 2013).

Mechanisms that have been used to explain the phase change in the annual cycle of precipitation do not distinguish between the response over land and ocean. As land and ocean differ in many ways, differentiating their phase responses is a natural next step towards understanding regional water cycle in a warming climate. In this study, we find that under global warming, the phase of tropical precipitation is delayed over land but advanced over ocean. Interestingly, despite covering only one-third of the Earth's surface, it is land, not ocean, that dominates the phase changes of zonal-mean precipitation annual cycle. The opposite phase changes between land and ocean will have profound implications for both terrestrial/marine ecosystems and human activities.

2. Data and methods

2.1 Model simulation data

Monthly mean data of multiple variables from 37 Coupled Model Intercomparison Project Phase 5 (CMIP5; Taylor et al. 2012) models and daily precipitation data from 40 members of CESM1 Large Ensemble (LENS) Project (Kay et al. 2015) are used in this study. The statistics of the present-day climate for 1962-2005 are from the historical (HIST) simulations while those for the future climate of 2056-2099 are from the RCP8.5 (RCP85) scenario simulations.

To examine the role of wind-evaporation-SST (WES) feedback on the phase changes of precipitation annual cycle, we also analyze two sets of experiments: one with the same fully coupled CESM1 as used for the CESM LENS Project and the other with a partially coupled configuration of CESM1 (Liu et al. 2018). Each set consists of a pair of 100-year long simulations with one under the condition of pre-industrial CO_2 (1xCO_2) and the other with CO_2 quadrupling (4xCO_2). In the partially coupled set, the wind speed from te pre-industrial simulation is prescribed through the bulk formula that is used to compute the evaporation over ocean in both the 1xCO_2 and 4xCO_2 runs, so that the part of the climate change response due to WES feedback is disabled. Comparing the response to 4xCO_2 forcing between the fully coupled and partially coupled sets allows the role of the WES feedback to be isolated. See Liu et al. (2018) for more details about the design of the experiments.

2.2 Phase estimated from the first Fourier harmonic

To estimate the phase of the annual cycle, Fourier transformation is performed to fit the related monthly time series to a Fourier harmonic (i.e., a sinusoidal function with time) with an angular frequency of $2\pi/12\text{mon}$. As the first Fourier harmonic explains more than 90% of variance in most models, we only use it to determine the phase of the annual cycle.

2.3 Atmospheric energetic framework

According to the atmospheric energy equation (Neelin and Held 1987), the divergence of AHT ($\nabla \cdot AHT$) is equal to the difference between the net energy input to the atmosphere F_{net} and the column moist static energy (MSE) tendency $\frac{\partial <h>}{\partial t}$:

$$\nabla \cdot AHT = F_{net} - \frac{\partial <h>}{\partial t}, \quad (1)$$

where the angle bracket represents vertical integration between the surface and the top of the model, F_{net} includes sensible heat flux, latent heat flux, net longwave radiation and net shortwave radiation, h is the MSE. Following Boos and Korty (2016), we also isolate the divergent component of the energy flux by solving the inverse Laplacian of energy flux potential χ, which is defined as

$$\nabla^2\chi = \nabla \cdot AHT \qquad (2)$$

3. Results

Figure 1 shows the future change in the annual cycle of tropical precipitation over land and ocean in both hemispheres. Climatologically, when the peak solar forcing moves across the equator from one hemisphere to another, tropical precipitation increases rapidly in the warmed hemisphere, but the timing of precipitation peak differs between land and ocean, with the former leading the latter by about a month due to its lower heat capacity (solid lines in Fig. 1a-d). Under global warming, there is an intriguing contrast in the future changes between land and ocean (bars in Fig. 1a-d): over land, precipitation anomalies peak much later than the climatological peak, while the opposite is true over ocean, indicating a phase delay in the precipitation annual cycle over land but a phase advance over ocean. The larger amplitude changes during the transition seasons over land than ocean accentuate the dominance of the land response in the zonal-mean response.

The phase changes over land versus ocean (0-40°N/S) are further quantified. Most CMIP5 models (Fig. 1e) and all LENS members (Fig. 1f) exhibit a seasonal delay over land, with median values of 2 to 4.5 days, and a seasonal advance over ocean, with a similar range of median values. For the Northern Hemispheric (NH) land and ocean, 34 and 33 out of 37 CMIP5 models show the phase delay and advance, respectively. Similarly for the Southern Hemispheric (SH) land and ocean, 36 and 29 out of 37 CMIP5 models show the phase delay and advance, respectively.

To decipher the contrasting precipitation phase changes between land and ocean, we conduct Empirical Orthogonal Function (EOF) analysis on the annual cycle of precipitation and identify two dominant modes (Fig. 2; Wang and Ding 2008): one characterized by an inter-hemispheric contrast (EOF1; accounting for 67.9% of variance) with a peak during local summer and the other featuring a distinct land-sea contrast (EOF2; accounting for 18.6% of variance) with a peak during local spring. Precipitation center tends to be well collocated with the local maxima of column MSE (contours in Figs. 2a-b). The phase change in both PCs is in quadrature to the phase of the corresponding climatological PCs, indicating a phase delay (Fig. 2c-d). The phase delay in the EOF1 has been attributed to both the phase delay in the annual cycle of SST and the annual-mean SST warming as explained above. The similar phase delays in PC1 and PC2 are mainly the result of EOF analysis that requires the EOF modes to be orthogonal to each other. The seasonal delay in both PC1 and PC2 is quite robust among the CMIP5 models and LENS simulations (Fig. 2e), with 36 out of 37 CMIP5 models and 39 out of 40 LENS members showing a delay. Another robust aspect in the response of the two EOF modes under warming is the enhancement of the amplitude in all CMIP5 models and LENS members, with a median increase of ~10% (Fig. 2f), consistent with the enhanced annual cycle of the global monsoon rainfall (Kitoh et al. 2013; Lee and Wang 2014).

Were the spatial pattern of the leading two EOF modes unchanged, the delay in their phases would imply a phase delay in the precipitation annual cycle over both land and ocean. But it turns out not to be the case (Fig. 1). As the two leading EOF modes of precipitation annual cycle explain more than 85% of the total seasonal variance, we construct the precipitation annual cycle over land and ocean (P_L and P_O, respectively) based on the two modes as follows:

$$P_L = A_{1,L} PC1 + A_{2,L} PC2 \quad (3)$$

$$P_O = A_{1,O}PC1 + A_{2,O}PC2 \quad (4)$$

Here, $PC1$ and $PC2$ are the corresponding normalized principle components, $A_{1,L}$ and $A_{2,L}$ are the amplitudes of EOF1 and EOF2 averaged over land, respectively; $A_{1,O}$ and $A_{2,O}$ are the same but over ocean.

Given the orthogonality of PCs, we can express the $PC1$ and $PC2$ as two sinusoidal functions with $PC2$ leading $PC1$ by $\pi/2$. Then, the annual cycle of P_L and P_O can be written as:

$$P_L = \sqrt{{A_{1,L}}^2 + {A_{2,L}}^2} sin\,(t - \phi_1 - \phi_L) \quad (5)$$

$$P_O = \sqrt{{A_{1,O}}^2 + {A_{2,O}}^2} sin\,(t - \phi_1 - \phi_O), \quad (6)$$

Here, t is time, ϕ_1 denotes the phase of PC1. It is found that the reconstructed precipitation annual cycle and the actual one is almost identical. This way, the phases of P_L and P_O are $\phi_1 + \phi_L$ and $\phi_1 + \phi_O$, respectively. $\phi_L = -\arcsin\left(\frac{1}{\sqrt{(\frac{A_{1,L}}{A_{2,L}})^2+1}}\right)$ and $\phi_O = \arcsin\left(\frac{1}{\sqrt{(\frac{A_{1,O}}{A_{2,O}})^2+1}}\right)$ represent extra phase associated with the relative contribution of EOF1 versus EOF2 to the land and ocean annual cycle, respectively. Under warming, if the amplitude of EOF1 increases more than EOF2 over land, $\frac{A_{1,L}}{A_{2,L}}$ becomes larger and the resultant change in ϕ_L would imply a delay. The opposite is true over ocean (note the opposite signs between ϕ_L and ϕ_O). The actual land-ocean phase change differences (Fig. 1e-f) can be well explained by their amplitude-based estimates (i.e., $\phi_L - \phi_O$), with correlation of 0.97 and 0.89 in NH and SH, respectively (Supplementary Fig. 1), lending support to the decomposition framework here. Hence, the land-sea difference in phase changes of precipitation annual cycles can also be casted in terms of the spatial pattern changes in EOF1 and EOF2 (i.e., $\frac{A_{1,L}}{A_{2,L}}$ and $\frac{A_{1,O}}{A_{2,O}}$).

Figure 3a shows a weak reduction in $\frac{A_{1,L}}{A_{2,L}}$, but a marked increase in $\frac{A_{1,O}}{A_{2,O}}$ in both hemispheres ($\frac{A_{1,O}}{A_{2,O}}$ increases by 38% and 29% for NH and SH, respectively) under warming, with the former opposing slightly the delay in ϕ_1 by an amount ϕ_L, while the latter overwhelming the positive change in ϕ_1, resulting in a net phase advance in P_O (i.e., $\phi_O + \phi_1 < 0$) shown in Fig. 1. Further examination indicates that the increase in $\frac{A_{1,O}}{A_{2,O}}$ is dominated by the increase in $A_{1,O}$ (Fig. 3b), with $A_{2,O}$ showing negligible changes (not shown). The change of EOF1 precipitation pattern (Fig. 3c) features large increases over broad tropical oceans, while the change is only marginal over tropical land, indicating a shift of precipitation from land to ocean during local summer when EOF1 peaks. This shift is robust in terms of the land-minus-ocean precipitation change among CMIP5 models (Supplementary Fig. 2a).

What tilts the land-ocean precipitation balance towards ocean in EOF1? As the "wet-get-wetter" response doesn't hold well over land due to the limited moisture supply (Fasullo 2012; Chadwick et al. 2013; Byrne and O'Gorman 2015; Donat et al. 2016), it may not be surprising that the land precipitation change is subdued relative to the ocean response. Here we explore other possible mechanisms via the energetic perspective. Viewing from the energetic constraint on precipitation, the land-ocean precipitation shift in EOF1 should be associated with an AHT from ocean to land, and indeed this is evidenced by the direct calculation of the change in AHT divergence contrast between land and ocean (Fig. 3c; Supplementary Fig. 2). This divergent flow of MSE appears to be from the warmer ocean to the colder land (Fig. 3c&d). According to the convective quasi-equilibrium argument suitable for the tropical convective regions (Emanuel

1995; Shekar and Boos 2016), the column MSE is approximately in equilibrium with the sub-cloud entropy, which is in turn regulated by the surface temperature (TS) when the surface relative humidity is high. With the diffusive nature of energy transport (Boos and Korty 2016), AHT should point from higher MSE to lower MSE regions and hence from the relatively warmer TS to the colder TS regions. The correlation between the land-sea contrast of AHT divergence and TS changes among CMIP5 models is 0.81 and 0.63 in NH and SH, respectively. Even over land, the corresponding correlation is 0.70 and 0.54, still statistically significant at 1% level. Previous studies (e.g., Hurley and Boos 2013; Roderick et al. 2014) suggested that over land, TS is mainly driven by precipitation when evaporation is limited. If so, the TS change would be negatively correlated with the change in precipitation and AHT divergence. Here, the significantly positive correlation between TS and AHT divergence changes over land implies the decreased TS over land does play a role in the suppressed precipitation in summer. As such, the land-sea precipitation shift during summer is linked to the opposite amplitude changes in the TS annual cycle over land and ocean, which is the focus of our investigation next.

Over ocean, a robust climate change response is the strengthening of surface wind in the winter subtropics and the weakening in the summer subtropics (Sobel and Camargo; contours in Fig. 3d). As wind speed is identified to be important in the tropical SST warming pattern formation (Xie et al. 2010), the contrasting wind response induces relative cooling in the winter subtropics and warming in the summer subtropics via WES feedback (Xie and Philander 1994; Lu and Zhao 2012), leading to the enhanced SST annual cycle (Fig. 3d). Thus, more rainfall occurs over ocean during summer, resulting in a phase advance over ocean. To further support our hypothesis, the CESM1 experiments with active WES reproduce the opposite phase changes of precipitation annual cycle over land and ocean (red crosses in Fig. 1f). When the WES feedback is disabled in the $4xCO_2$ experiments, the phase advance over ocean is completely nullified in NH and reduced by more than half in SH, whereas the land phase delay mostly persists (blue crosses in Fig. 1f).

In contrast to the increased amplitude of TS over ocean, the amplitude of TS is reduced over land, most notably in the monsoon regions (Fig. 3d). The governing mechanism for the annual cycle of temperature over land can be captured by an atmosphere-land surface interaction model forced by a periodic solar insolation:

$$C_A \frac{dT_A}{dt} = \lambda(T_S - T_A) - \mathrm{B}\, T_A \tag{7}$$

$$C_S \frac{dT_S}{dt} = -\lambda(T_S - T_A) + R, \tag{8}$$

where T_A is the mass-weighted temperature of the column atmosphere, which is dominated by the near surface air temperature, T_s is the land TS, C_A and C_S are the effective heat capacities of the atmosphere and surface, respectively. The total surface-atmosphere energy exchange including longwave radiation, sensible and latent heat fluxes is parameterized to be linearly proportional to $T_S - T_A$ with an exchange coefficient λ (as similarly treated in Barsugli and Battisti (1998) and Zhou and Xie (2018)). B is the bulk feedback parameter accounting for all the radiative processes at the top of atmosphere, including water vapor, cloud, lapse rate and Planck feedbacks. Since the adjustment of T_A through the top of the atmosphere is slower than that at the surface, B is generally smaller than λ (Barsugli and Battisti 1998). The system is forced at the surface by a periodic solar radiation R with a frequency of yr^{-1}, hence shortwave absorption by the atmosphere is neglected.

Over tropical land, C_S is estimated to be one order smaller than C_A. Thus, adding Eqs. (7) and (8) together and ignoring the small term associated with C_S reduce the system to a single variable system:

$$C_A \frac{dT_A}{dt} = -\mathrm{B}T_A + R, \tag{9}$$

from which the amplitude relation between T_A and R can be derived:

$$|T_A| = \frac{|R|}{\sqrt{\mathrm{B}^2 + \omega^2 {C_A}^2}}, \tag{10}$$

where $\omega = 2\pi\, yr^{-1}$. Under the condition $\omega C_A \ll \lambda$, which holds well for the modern climate condition, the amplitude relation between T_A and T_S can be written as:

$$|T_S| \approx (1 + \frac{B}{\lambda})|T_A|, \tag{11}$$

Thus, for a given solar insolation, the amplitude of atmospheric temperature decreases with the increase in the effective atmospheric heat capacity and bulk feedback parameter B. The same may also be said of the amplitude of T_S considering the linear relationship between T_S and T_A from Eq. (11).

Following Schwartz (2007), the effective atmospheric heat capacity is defined as $C_A = \frac{\partial <h>/\partial t}{\partial <T>/\partial t}$, with $< h >$ and $< T >$ representing the vertically-integrated MSE and temperature. This definition of C_A allows to estimate it by regressing the monthly tendency of multi-model ensemble mean $< h >$ against that of $< T >$. Based on this definition, C_A can be scaled as $C_A \approx c_p + \frac{L_v <q>}{<T>}$, where $< q >$ is the vertically integrated water vapor. As $< q >$ increases nonlinearly with temperature following the Clausius-Clapeyron relation, C_A increases as the mean climate warms. Song et al. (2018a) has already shown that the annual cycle of $\partial < h >/\partial t$ is robustly enhanced mainly due to the contribution from $\partial < L_v q >/\partial t$, which scales linearly with global warming. Here, we provide further evidences for the increase of effective atmospheric heat capacity (Supplementary Fig. 3). In the current climate, C_A is 2162.10 and 2704.01 J kg^{-1} K^{-1} for NH and

SH, respectively. Under global warming, C_A is increased to 2393.10 and 3271.39 J kg^{-1} K^{-1}, with an increase rate of 10.7% and 21.0% for NH and SH, respectively. The enhancement of C_A is ubiquitous across all CMIP5 models examined (Supplementary Fig. 4). As no robust change in B is found over tropical land under warming in CMIP5 models, the robust increase of the effective atmospheric heat capacity acts to reduce the amplitude of the T_A and T_s annual cycle over land, consistent with Cronin and Emanuel (2013) based on radiative-convective equilibrium simulations.

Since a good proportionality holds between T_A and T_S with small phase differences for the system above, we can further simplify Eq. (8) into a surface energy balance model for T_s:

$$C_S \frac{dT_s}{dt} = -\beta T_s + R, \quad (12)$$

where β is a parameter to measure the surface cooling feedback, encompassing processes of net longwave radiative cooling and turbulent heat fluxes. A similar surface energy model has been used to understand the temperature annual cycle in an extraterrestrial planet (Mitchell et al. 2014), where only longwave radiation is considered in the damping term. The amplitude of T_s governed by Eq. (12) is determined by

$$|T_s| = \frac{|R|}{\sqrt{\beta^2 + \omega^2 {C_S}^2}}, \quad (13)$$

and is expected to decrease with an increase of the feedback parameter β. We estimate β by regressing the total surface energy flux excluding the shortwave fluxes on the annual cycle of TS for both current and future climates. The resultant β is generally positive over land in the current climate (Supplementary Fig. 5a), vindicating its physical meaning as a damping parameter. In the tropical monsoonal regions, β indeed increases across the majority of CMIP5 models under the

RCP85 scenario and geographically, it coincides with regions of decreased TS annual cycle (Fig. 3d and Supplementary Fig. 5b). Averaged over the land monsoonal regions, the change of β is significantly (at 1% level) correlated with that of summer-vs-winter TS difference across the CMIP5 models, with correlations reaching -0.68 in NH and -0.46 in SH (or -0.81 with the outlier models excluded) (Supplementary Fig. 6). Taken together, both the increase of C_A and β work in tandem to dampen the TS amplitude over land.

4. Conclusions

This study discovers intriguing opposite phase changes in the precipitation annual cycle between land and ocean under climate warming: a delay over land, but an advance over ocean. Although land only covers one-third of the Earth's surface, it dominates the phase delay of zonal-mean precipitation annual cycle previously found (Biasutti and Sobel 2009; Song et al. 2018a). The delay over land is mainly determined by the increased effective atmosphereic heat capacity under warming, the same mechanism responsible for the zonal-mean precipitation delay (Song et al. 2018a). The phase advance over ocean is related to a shift of precipitation center towards ocean in the local summer, which overwhelms the phase delay resulting from the increased effective atmospheric heat capacity. The shift of precipitation from land to ocean during the peak rainy season corresponds well to the pattern of AHT divergence change, epitomizing the energetic constraint on the tropical precipitation change even at the regional scale. The AHT divergence change under climate warming is closely related to the opposite changes in the amplitude of TS annual cycle between land and ocean. The strengthened surface wind in winter cools SST and the weakened one in summer warms SST, enhancing the amplitude of SST annual cycle. Over land, on the other hand, both the increased effective atmospheric heat capacity and surface cooling feedback over monsoonal regions act to dampen the amplitude of TS annual cycle. The combination of enhanced TS amplitude over ocean and reduced TS amplitude over land rebalances the atmospheric column energy in favor of ocean precipitation. As a result, the center of precipitation shifts towards ocean, which is further manifested as a differential phase change between land and ocean.

Considering the earlier transition from dry to wet seasons over land than ocean in the climatological annual cycle, the phase delay over land and phase advance over ocean under warming will make the two more in sync in a warmer future. The delayed onset of rainfall as well as the dampened annual cycle of temperature over land would have profound economic and societal impacts, especially for regions like Asia, Africa and Latin America, where the local rainfed agriculture and economy are under the sway of monsoonal rain.

Acknowledgement

This research is supported by the U.S. Department of Energy Office of Science Biological and Environmental Research as part of the Regional and Global Modeling and Analysis program area. PNNL is operated for the Department of Energy by Battelle Memorial Institute under contract DE-AC05-76RL01830. We acknowledge the World Climate Research Program's Working Group on Coupled Modeling, which makes CMIP5 data available (http://www.ipcc-data.org/sim/gcm_monthly/AR5/Reference-Archive.html) and NCAR CESM1 group, which makes the large-ensemble (LENS) experiments available (http://www.cesm.ucar.edu/projects/community-projects/LENS/).

References

Barsugli, J. J. and D. S. Battisti (1998), The basic effects of atmosphere-ocean thermal coupling on midlatitude variability. J. Atmos. Sci. 55, 477–493.

Biasutti, M. and A. H. Sobel (2009), Delayed Sahel rainfall and global seasonal cycle in a warmer climate. *Geophys. Res. Lett.,* 36, L23707.

Biasutti, M., A. Voigt, W. R. Boos, P. Braconnot, J. C. Hargreaves, S. P. Harrison, et al (2018), Global energetics and local physics as drivers of past, present and future monsoons. *Nature Geoscience* 11(6), 392-400.

Boos, W. R. and R. L. Korty (2016), Regional energy budget control of the intertropical convergence zone and application to mid-Holocene rainfall. *Nat. Geosci.* 9, 892–897.

Byrne, Michael P. and Paul A. O'Gorman (2015), The Response of Precipitation Minus Evapotranspiration to Climate Warming: Why the "Wet-Get-Wetter, Dry-Get-Drier" Scaling Does Not Hold over Land. Journal of Climate 28, 8078-8092.

Chadwick, R., I. Boutle, and G. Martin, (2013) Spatial patterns of precipitation change in CMIP5: why the rich do not get richer in the tropics. *J. Clim.* 26, 3803–3822.

Chou, C., J.-Y. Tu and P.-H. Tan (2007), Asymmetry of tropical precipitation change under global warming. *Geophys. Res. Lett.* 34, L17708.

Chou, C., J. Neelin, C. Chen and J. Tu (2009), Evaluating the 'rich-get-richer' mechanism in tropical precipitation change under global warming. *J. Clim.* 22, 1982–2005.

Chou, C. and C-W. Lan (2012), Changes in the annual range of precipitation under global warming. *J. Clim.* 25, 222–235.

Cronin, T. W. and K. A. Emanuel (2013), The climate time scale in the approach to radiative-convective equilibrium. *J. Adv. Model. Earth Syst.* 5, 843–849 (2013).

Donat, M. G., A. L. Lowry, L. V. Alexander, P. A. O'Gorman and N. Maher (2016) More extreme precipitation in the world's dry and wet regions. *Nat. Clim. Change* 6, 508–513.

Donohoe, A. and D. S. Battisti (2013),The seasonal cycle of atmospheric heating and temperature. *J. Clim.* 26, 4962–4980.

Dwyer, J. G., M. Biasutti and A. H. Sobel (2012), Projected changes in the seasonal cycle of surface temperature. *J. Clim.* 25(18), 6359–6374.

Dwyer, J. G., M. Biasutti and A. H. Sobel (2014), The effects of greenhouse gas-induced changes in SST on the annual cycle of zonal mean tropical precipitation. *J. Clim.* 27, 4545-4565.

Emanuel, K. A. (1995), On thermally direct circulation in moist atmosphere. J. Atmos. Sci. 52, 1529-1534.

Fasullo, J. (2012), A mechanism for land–ocean contrasts in global monsoon trends in a warming climate. *Clim. Dynam.* 39, 1137–1147.

Frierson, D. M. W. et al (2013), Contribution of ocean overturning circulation to tropical rainfall peak in the northern hemisphere. *Nature Geosci.* 6, 940–944.

Held, I. M. and B. J. Soden (2006), Robust responses of the hydrological cycle to global warming. *J. Clim.* 19, 5686–5699.

Huang, P., S-P. Xie, K. Hu, G. Huang and R. Huang (2013), Patterns of the seasonal response of tropical rainfall to global warming. *Nature Geosci.* 6, 357–361.

Hurley, J. V., and W. R. Boos (2013), Interannual variability of monsoon precipitation and subcloud equivalent potential temperature, J. Climate, 26, 9507–9527.

Kang, S. M., I. M. Held, D. Frierson and M. Zhao (2008), The response of the ITCZ to extratropical thermal forcing: Idealized slab-ocean experiments with a GCM. *J. Clim.* 21(14):3521–3532.

Kay, J. E. et al (2015), The Community Earth System Model (CESM) Large Ensemble Project: A Community Resource for Studying Climate Change in the Presence of Internal Climate Variability, *Bull. Am. Meteorol. Soc.* 96, 1333-1349.

Kitoh, A. et al (2013), Monsoons in a changing world: a regional perspective in a global context. *J. Geophys. Res.* 118, 3053–3065.

Lee, J.-Y. and B. Wang (2014), Future change of global monsoon in the CMIP5. *Clim Dynam* 42, 101–119.

Liu, W., J. Lu, S. P. Xie and A. Fedorov (2018), Southern Ocean heat uptake, redistribution, and storage in a warming climate: The role of meridional overturning circulation. *J. Clim.* 31, 4727–4743.

Lu, J. and B. Zhao (2012), The role of oceanic feedback in the climate response to doubling CO2. *J. Clim.* 25, 7544–7563.

Mitchell, J. L., G. K. Vallis, and S. F. Potter (2014), Effects of the Seasonal Cycle on Superrotation in Planetary Atmospheres, The Astrophysical Journal 787(1), 23.

Neelin, J. and I. M. Held (1987), Modeling tropical convergence based on the moist static energy budget. Mon. Wea. Rev. 115, 3–12.

Pascale, S., V. Lucarini, X. Feng, , A. Porporato & S. Hasson (2016), Projected changes of rainfall seasonality and dry spells in a high greenhouse gas emissions scenario. *Clim. Dyn.* 46, 1331–1350.

Roderick, M. L., F. Sun, W. H. Lim, and G. D. Farquhar (2014), A general framework for understanding the response of the water cycle to global warming over land and ocean. Hydrol. Earth Syst. Sci., 18, 1575–1589.

Schneider, T., T. Bischoff and G. H. Haug (2014), Migrations and dynamics of the intertropical convergence zone. *Nature* 513, 45–53.

Schwartz, S. E. (2007), Heat capacity, time constant, and sensitivity of Earth's climate system. *J. Geophys. Res.* 112, D24S05.

Seth, A., S. A. Rauscher, M. Rojas, A. Giannini and S. J. Camargo (2011), Enhanced spring convective barrier for monsoons in a warmer world? *Climatic Change* 104, 403–414.

Seth, A. et al. (2013), CMIP5 projected changes in the annual cycle of precipitation in monsoon regions. *J. Clim.* 26, 7328–7351.

Shekar, R. and W. R. Boos (2016), Improving energy-based estimate of monsoon location in the presence of proximal desert. J. Clim. 29, 4741-4761.

Sobel, A. H. and S. J. Camargo (2011), Projected future changes in tropical summer climate. *J. Clim.* 24, 473–487.

Song, F., L. R. Leung, J. Lu and L. Dong (2018a), Seasonally dependent responses of subtropical highs and tropical rainfall to anthropogenic warming. *Nature Clim. Change* 8, 787–792.

Song, F., L.R. Leung, J. Lu and L. Dong (2018b), Future changes in seasonality of the North Pacific and North Atlantic subtropical highs, *Geophysical Research Letters*, 45, 11,959-11,968.

Taylor, K. E., R. J. Stouffer, and G. A. Meehl (2012), An overview of CMIP5 and the experiment design. *Bull. Am. Meteorol. Soc.* 93, 485–498.

Wang, B. and Q. Ding (2008), Global monsoon: Dominant mode of annual variation in the tropics. *Dynam Atmos Oceans* 44, 165–183.

Xie, S. P. and S. G. H. Philander (1994), A coupled ocean-atmosphere model of relevance to the ITCZ in the eastern Pacific. *Tellus A* 46, 340–350.

Xie, S. P. et al. (2010), Global warming pattern formation: Sea surface temperature and rainfall. *J. Clim.* 23, 966–986.

Zhou, W., and S. P. Xie (2018), A Hierarchy of Idealized Monsoons in an Intermediate GCM, *J. Clim.* 31(22), 9021–9036.

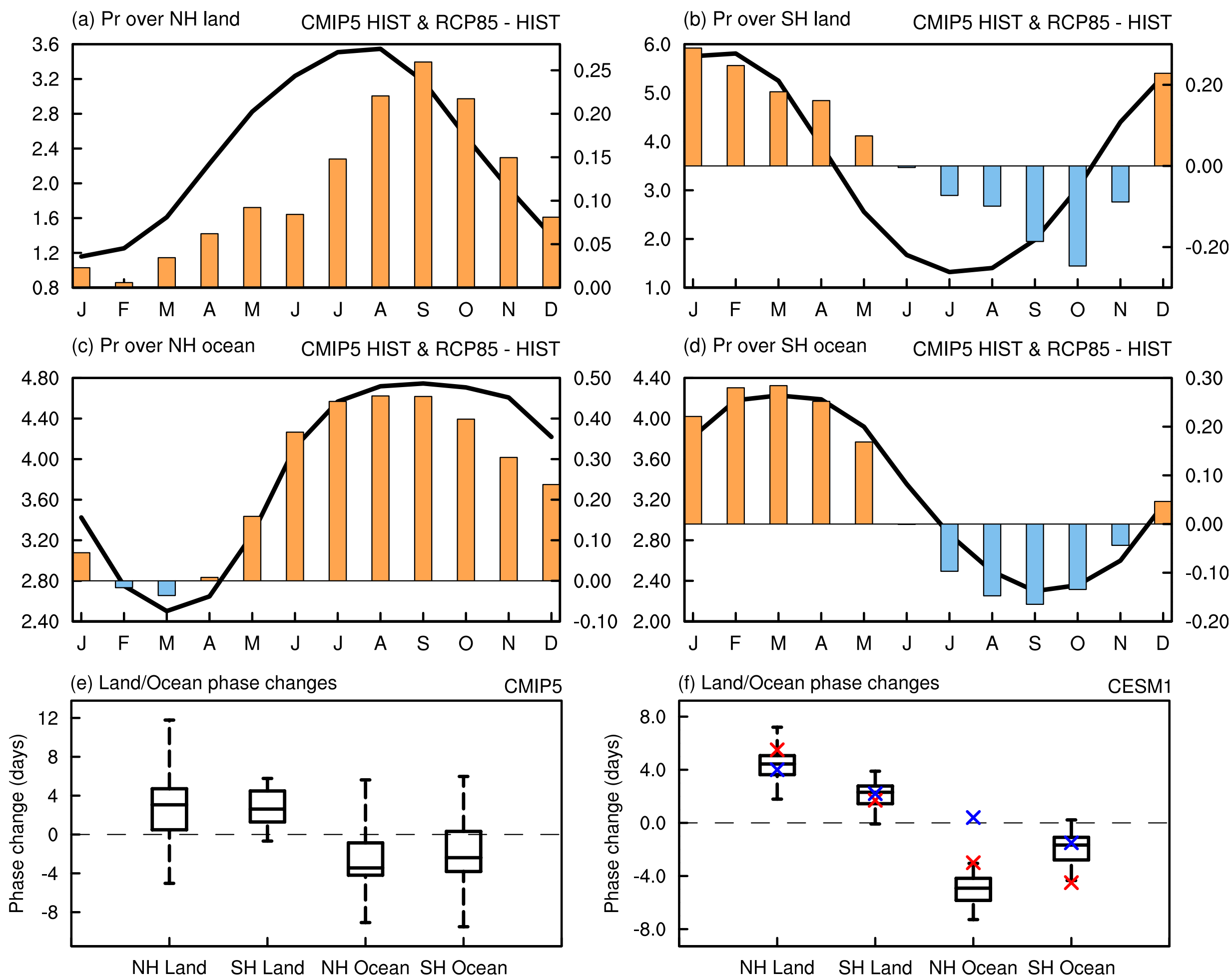

Figure 1 The annual cycle of precipitation (unit: mm day^{-1}) in HIST runs (black line) and its future changes between RCP85 and HIST runs over (a) North Hemispheric (NH) land (0°-40°N), (b) South Hemispheric (SH) land (0°-40°S), (c) NH ocean (0°-40°N) and (d) SH land (0°-40°S). Box-plots for the future phase changes in the precipitation annual cycle over land and ocean from (e) CMIP5 monthly data and (f) CESM1 LENS daily data. The lines in each box represent the 25th percentile, median, and the 75th percentile, and the whiskers represent the minimum and maximum of the multi-model (or LENS) ensemble. In (f), the red and blue crosses indicate the phase changes between the 4xCO_2 and 1xCO_2 experiments of CESM1 with and without WES feedback, respectively.

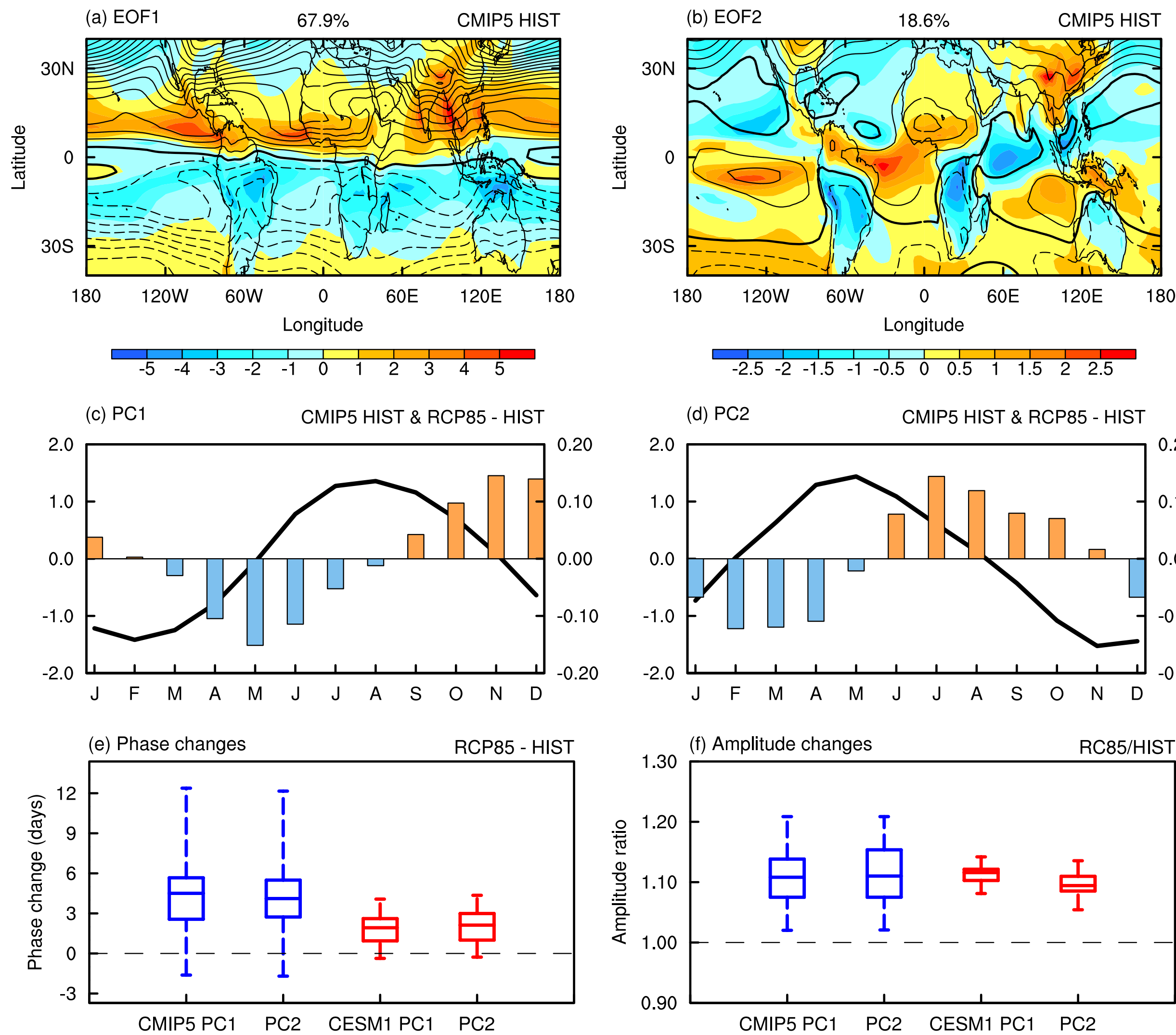

Figure 2 The spatial patterns of (a) EOF1 and (b) EOF2 in HIST runs and the corresponding normalized principle components (c) PC1 and (d) PC2 in HIST (black line) and their corresponding future changes between RCP85 and HIST. In a (b), overlaid as contours is the vertically-integrated MSE (unit: 10^7 J kg^{-1}) regressed upon the normalized PC1 (PC2) in HIST runs. The bold line indicates zero and solid (dashed) lines represent positive (negative) values with an interval of 0.5×10^7 J kg^{-1}. Box-plots for (e) the phase changes and (f) the amplitude ratio between RCP85 and HIST for the two EOF modes from CMIP5 (blue) and CESM1 LENS (red).

The lines in each box represent the 25th percentile, median, and the 75th percentile, and the whiskers represent the minimum and maximum of the multi-model (or LENS) ensemble.

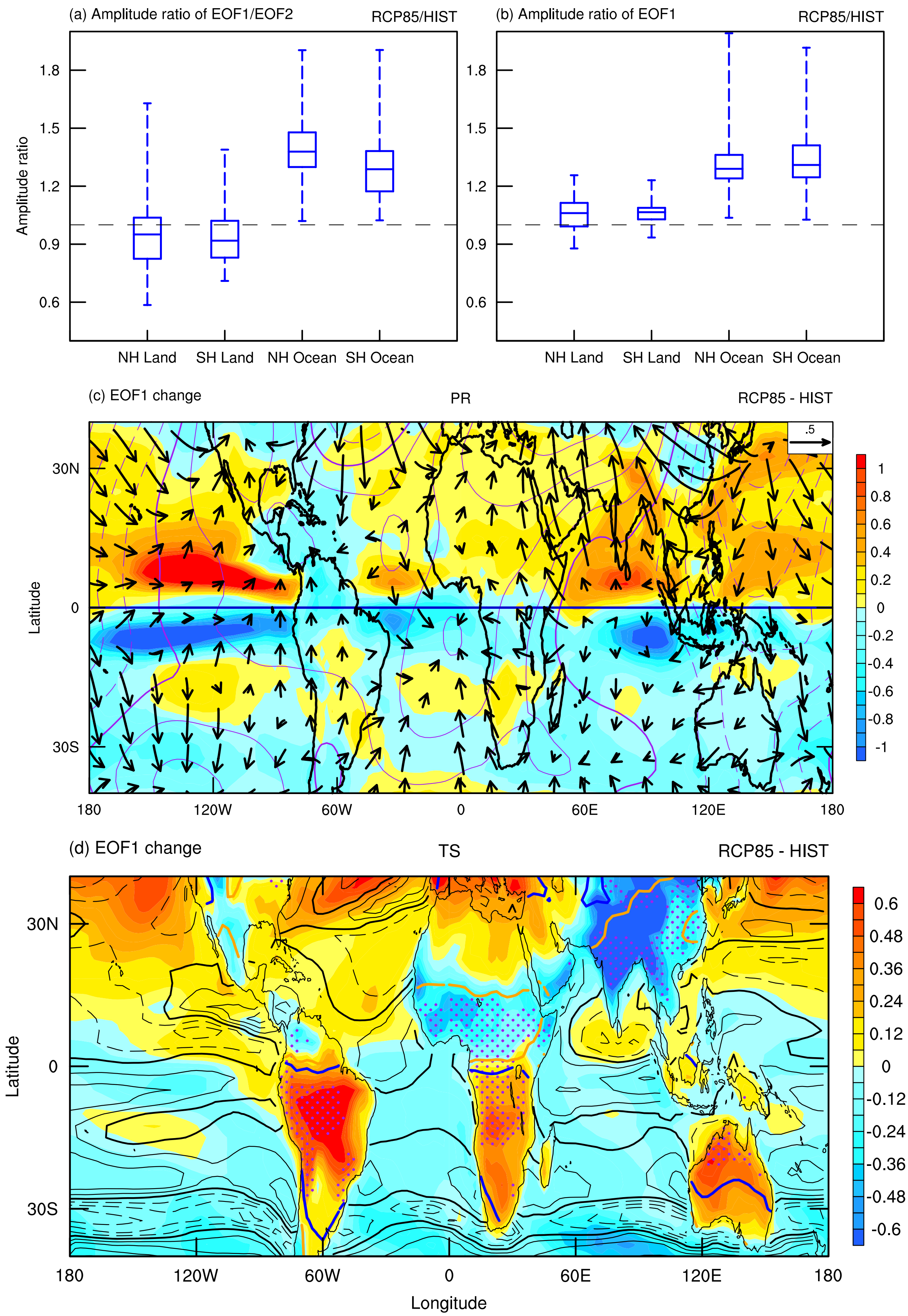
(a) Amplitude ratio of EOF1/EOF2
RCP85/HIST
Amplitude ratio
1.8
1.5
1.2
0.9
0.6
NH Land
SH Land
NH Ocean
SH Ocean
(b) Amplitude ratio of EOF1
RCP85/HIST
(c) EOF1 change
PR
RCP85 - HIST
.5
30N
0
30S
Latitude
180
120W
60W
60E
120E
1
0.8
0.6
0.4
0.2
-0.2
-0.4
-0.6
-0.8
-1
(d) EOF1 change
TS
RCP85 - HIST
0.6
0.48
0.36
0.24
0.12
-0.12
-0.24
-0.36
-0.48
-0.6
Longitude

Figure 3 Box-plots comparing the ratio of the amplitude of (a) EOF1 over land $A_{1,L}$ divided by EOF2 over land $A_{2,L}$ and EOF1 over ocean $A_{1,O}$ divided by EOF2 over ocean $A_{2,O}$ and (b) EOF1 over land $A_{1,L}$ and EOF1 over ocean $A_{1,O}$ between the RCP85 and HIST runs (i.e., RCP85 divided by HIST) among CMIP5 models. Future change of (c) precipitation (shaded; unit: mm day^{-1}), energy flux potential (contour; unit: W) and divergent energy flow (vectors; unit: 10^7 W m^{-1}) and (d) TS (unit: K) regressed on the PC1 of precipitation annual cycle between the RCP85 and HIST runs. In c, the bold line is zero and the solid (dashed) contours denote positive (negative) values with the contour interval of $0.4x10^{13}$ W. The line patterns over ocean in d have the same meaning as c except that it is the change in the 1000 hPa wind speed congruent with EOF1 and the interval is 0.2 m s^{-1}. The orange and blue contours over land in d indicate the 0.5 and -0.5 mm day^{-1} contours of precipitation EOF1 shown in Fig. 2a, respectively, demarcating the boundaries of the land monsoonal regions. The purple dots over land indicate regions of increased surface cooling feedback parameter β under global warming. The horizontal lines in a and b represent the minimum, 25th percentile, median, 75th percentile, and the whiskers are the maximum and minimum values of the multi-model ensemble.